CompositesAI™

Resolving the single-ply woven plate bending mismatch: a multi-agent study led by CompositesAI with OpenSG and Abaqus

Technical report

Akshat Bagla Wenbin Yu
Purdue University, West Lafayette, IN, USA

October 2026

Abstract

A cdmHUB forum question asks whether reference-point coupling explains why the plate bending stiffness of a single thin plain-weave ply, modelled by a structure genome (SG), is about 27 % of that from classical lamination theory (CLT) with 3-D constants and about 25 % of that from Abaqus. We investigated the cdmHUB thin plain-weave plate discrepancy by benchmarking OpenSG homogenization and Abaqus direct numerical simulation on the same heterogeneous voxel SG with identical constituent properties and per-element yarn orientations. After identifying that the supplied SG contains two in-phase fabric layers and extracting the true single layer, we found that the single-layer Kirchhoff plate model gives substantially lower bending stiffness than CLT reconstructed from 3-D periodic-solid constants, while the gap closes rapidly as additional layers are stacked. Abaqus periodic-cell and coupon bending simulations reproduced the low single-layer plate stiffness, and in this benchmark reference-point coupling changed it by only a few percent, indicating that the forum-scale discrepancy is not caused by coupling boundary conditions alone but is more plausibly related to SG definition, thickness interpretation, constitutive idealization, discretization, or stiffness extraction. Each prospective cause is listed with its symptom and check.

1 Introduction

The mechanics of structure genome (MSG) can homogenize a textile composite either as a 3-D solid, using a structure genome (SG) treated as periodic in all three directions, or directly as a plate, using an SG that is periodic in-plane with traction-free top and bottom faces [1–3]. For laminates with many repeating fabric layers, the two routes can give similar in-plane stiffnesses and, in favourable cases, similar plate stiffnesses; for a single thin fabric layer they need not, because they are different boundary-value problems.

The cdmHUB forum question [4] reports such a case: a single thin plain-weave ply, thickness $t = 0.0667$ mm, analysed with SwiftComp. The 3-D solid SG gives $E_1^{3D} = 81.86$ GPa; the Kirchhoff plate SG gives, inferred from its extensional stiffness matrix $\mathbf{A}$, $E_1^A = 68.70$ GPa. In bending, the plate SG gives $D_{11}^{\text{plate}} = 0.55$ N mm, whereas classical lamination theory (CLT) with the 3-D constants gives $D_{11}^{\text{CLT}} = 2.03$ N mm, and an Abaqus model with each end face coupled to a reference point and no periodic boundary conditions gives 2.17 N mm. As reported in the cdmHUB forum discussion, as the number of plies increases, the plate results move toward the 3-D-solid-based values. The reply on the forum attributes the difference to the constraints: the 3-D SG is periodic in all three directions, the plate SG only in-plane, with free top and bottom faces. The follow-up question remained open: can the reference-point coupling of the Abaqus model explain a bending stiffness about four times the plate value? In terms of the membrane ratio $R_E = E_1^A/E_1^{3D}$ and the bending ratio $R_D = D_{11}^{\text{plate}}/D_{11}^{\text{CLT}}$ (Eq. (1)), the values reported on cdmHUB give $R_E = 0.839$ and $R_D = 0.271$. Here D_{11}^{CLT} (Eq. (2)) is only a diagnostic reconstruction from the 3-D periodic-solid constants, not the physical reference for a single layer with free faces.

These two queries, whether the low single-ply plate D_{11} is real and whether reference-point coupling in Abaqus explains the factor of about four, started the present study. Its purpose is to resolve the mismatch and to identify modelling causes that a user can check. CompositesAI [5] led the study: planning, specification of the models and boundary conditions, interpretation of the results and review. OpenSG [6] performed the MSG homogenization and Abaqus/Standard [7] the direct numerical simulation; Claude Code served as the agentic distribution channel, dispatching the tasks to computational agents and relaying queries and results (Fig. 1).

This report addresses the follow-up question for a crimped plain-weave SG of the same kind, not for the unavailable SG used in the forum post. It is a mechanistic benchmark on the supplied plain-weave SG of Rouf, Liu and Yu [3]; its fabric layer is 0.02 mm thick instead of 0.0667 mm, so the comparison is made through R_E and R_D, not through absolute values. The objectives are (i) to establish whether a low single-layer plate D_{11} is a property of a fabric layer with free faces or an artefact of the homogenization; (ii) to test whether the boundary conditions of a reference-point-coupled Abaqus model can raise D_{11} about fourfold; and (iii) to list the modelling choices that can produce such a gap, each with the symptom it leaves and the check that exposes it.

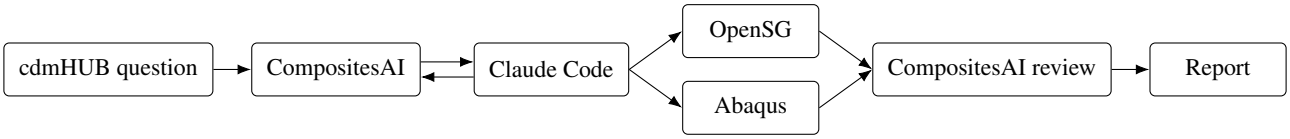
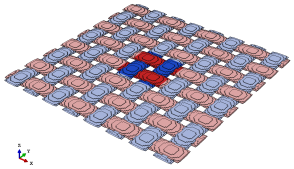
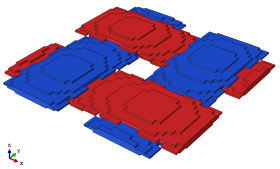


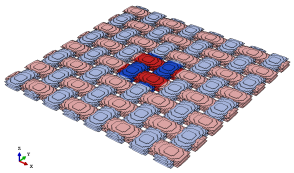
Figure 1: Workflow: CompositesAI led the study; Claude Code distributed its tasks to agents running OpenSG and Abaqus; CompositesAI reviewed the results and the report.



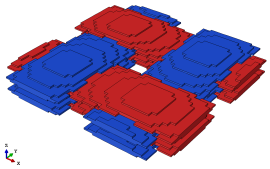
(a) Single-layer plate, 4×4 cells, extracted cell highlighted



(b) Single-layer SG



(c) Two-layer plate, 4×4 cells (illustration), extracted cell highlighted



(d) Two-layer SG (as supplied)

Figure 2: SG extraction: genuine Abaqus/CAE model views with the matrix hidden; warp tows red (fibre along x), weft tows blue (fibre along y). Plates $1.2 \times 1.2 \times 0.02$ mm (a) and $1.2 \times 1.2 \times 0.04$ mm (c); SGs $0.3 \times 0.3 \times 0.02$ mm (b) and $0.3 \times 0.3 \times 0.04$ mm (d).

Section 2 shows that the published 0.04 mm SG is an in-phase stack of two identical 0.02 mm fabric layers, which a 3-D solid homogenization periodic in x_3 does not distinguish from one repeating layer, and extracts the single layer. Section 3 explains why plate and 3-D solid homogenization are different boundary-value problems and shows that the single layer reproduces the forum trend, whereas the two-layer SG does not. Section 4 bends the same heterogeneous layer in Abaqus and specifies, for every model, the element type, periodic constraints, load or curvature prescription, edge conditions, reference-point coupling and the formula used to extract D_{11}: periodic cells, free-edge coupons and reference-point-coupled coupons all return the low plate D_{11}, and in this benchmark the coupling changes it by only a few per cent. Section 5 identifies the likely classes of modelling choices responsible for the forum-scale gap, each with its symptom and the check that exposes it, and Section 6 concludes.

2 Structure genome

Geometry and materials. The SG is a voxel model of the plain-weave example of Rouf et al. [3]: 0.3×0.3 mm in the x_1–x_2 plane and 0.04 mm thick along x_3, discretized into $40 \times 40 \times 16$ eight-node hexahedra of $7.5 \times 7.5 \times 2.5$ µm (28 577 nodes, 25 600 elements), with $x_1, x_2 \in [-0.075, 0.225]$ mm. Warp tows run along x_1 and weft tows along x_2, 6688 elements each; the voxelized tow volume fraction, computed as tow elements over all elements, is 0.5225; the matrix occupies the remainder. Each tow element has its own material frame with local axis 1 aligned to the local yarn path, so the fibre direction follows the crimp; the maximum local inclination of the yarn axis to the mid-plane, measured from the element frames of the SG, is 5.7°. In all 3584 tow elements checked per family, the sign of the out-of-plane fibre component agrees with the slope of the yarn centreline. Table 1 lists the constituents. The tow material is orthotropic in the yarn frame. Although $E_2 = E_3$ and $G_{12} = G_{13}$, it is not transversely isotropic because $G_{23} = 3.22\,\text{GPa} \neq E_2/[2(1+\nu_{23})] = 5.73\,\text{GPa}$.

Table 1: Constituent properties in the yarn frame (axis 1 along the fibre). The matrix is isotropic; its shear modulus is $E/[2(1+\nu)]$.

Property	Tow	Matrix
E_1 (GPa)	126.91	4.51
$E_2 = E_3$ (GPa)	16.49	4.51
$G_{12} = G_{13}$ (GPa)	3.72	1.63
G_{23} (GPa)	3.22	1.63
$\nu_{12} = \nu_{13}$	0.26	0.38
ν_{23}	0.44	0.38

The SG holds two fabric layers. If the 0.04 mm SG is interpreted as one ply, as in the forum question, the plate comparison is misleading. Four observations show that it is an in-phase stack of two identical 0.02 mm layers: (i) the x_1–x_3 section (Fig. 3) shows one warp tow in each half, separated by matrix at mid-thickness; (ii) in every through-thickness column of 16 elements each tow family appears either twice, once in each half, or not at all (1072 and 528 of the 1600 columns for each family); (iii) the bottom and top halves, eight element layers each, are identical element by element: the same material in all 12 800 element pairs and the same local frames to machine precision; (iv) no column has tow on both sides of the mid-plane, so no tow crosses it. This is consistent with the source publication, which describes its plate-like structure as two plies of plain-weave fabric, 0.02 mm each [3]. The published SG and its 3-D solid homogenized properties are therefore internally consistent; the issue arises only if that 0.04 mm SG is interpreted as a single fabric layer. For the present SG, a 3-D solid homogenization periodic in x_3 does not distinguish the full SG from either half repeated through the thickness: the 3-D stiffness matrix $\mathbf{C}$ of the bottom half equals that of the full SG to a relative difference of 7×10^{-17}. Only a model with free top and bottom faces, such as the plate SG, distinguishes one layer from two.

The single layer. The single fabric layer used in this study, called the true single layer below, is taken as the bottom half (lower eight voxel layers) of the published SG: $0.3 \times 0.3 \times 0.02$ mm, $40 \times 40 \times 8$ elements (15 129 nodes, 12 800 elements), with the original voxel materials and local frames preserved, so the voxelized tow volume fraction stays 0.5225. It is re-centred so that $x_3 \in [-0.01, 0.01]$ mm, and $h = 0.02$ mm is the thickness in every single-layer plate,

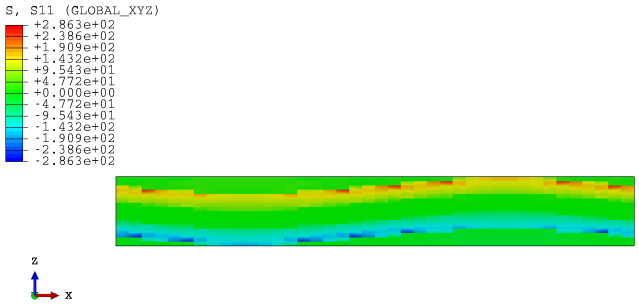


Figure 3: The supplied SG, $0.3 \times 0.3 \times 0.04$ mm, in Abaqus/CAE: x_1–x_3 section through a warp tow, axial stress S_{11} (MPa) under periodic cylindrical bending (periodic in x_1 and x_2), $\kappa_{11} = 0.1\ \mathrm{mm}^{-1}$, $\kappa_{22} = 0$, top and bottom faces traction-free; C3D8 elements, 16 through the thickness; deformation scale factor 0.3. Each 0.02 mm half contains a distinct warp-tow pass.

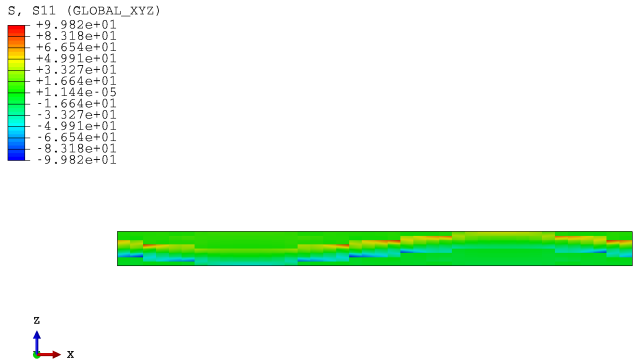


Figure 4: The true single layer, $0.3 \times 0.3 \times 0.02$ mm (bottom half of the supplied SG), in Abaqus/CAE: x_1–x_3 section through the same warp tow as in Fig. 3, S_{11} (MPa) under the same loading and boundary conditions; C3D8 elements, 8 through the thickness; deformation scale factor 0.3.

CLT and Abaqus calculation. Warp and weft tows interlace within this thickness. Under the same bending, S_{11} changes sign through the thickness of the individual crimped tow (Fig. 4), consistent with bending of one crimped fabric layer. Fig. 2 shows each SG as the central cell of a plate of 4×4 cells: the single layer (a, b) and, for comparison, the two-layer SG (c, d). This layer is the SG of Sections 3 and 4; the two-layer SG is kept as a reference. With the SG established, the next section contrasts the two homogenization problems applied to it.

3 Plate versus 3-D solid homogenization

3.1 Two boundary-value problems

Both homogenizations use OpenSG, an open-source implementation of MSG [1, 6] (commit f31b196), on the same voxel mesh, materials and element frames. The *3-D solid SG* is periodic in x_1, x_2 and x_3; it returns the 6×6 stiffness matrix $\mathbf{C}$ and the engineering constants E_1^{3D}, ν_{12}, ... of a material point. The *classical (Kirchhoff–Love) plate SG* is periodic in x_1 and x_2 only, its top and bottom faces are traction-free, and it returns the membrane, coupling and bending matrices $\mathbf{A}$, $\mathbf{B}$, $\mathbf{D}$ about the mid-plane for the plate strains and curvatures.

The two homogenization problems admit different admissible local fields. The 3-D SG represents a material point inside an infinite stack of identical layers; periodicity in x_3 restricts the free-surface relaxation modes that a finite-thickness layer has. The plate SG represents the whole layer with free faces and admits these modes. For this crimped plain-weave SG they reduce the membrane stiffness and, more strongly, the bending stiffness, for which the plate energy weights distance from the mid-plane by x_3^2 (Table 2). The fraction of material influenced by the free faces grows as the layer thins, so the gap is largest for one layer and decreases as layers are stacked [2] (Table 3).

The comparison uses the membrane and bending ratios

$$R_E = \frac{E_1^A}{E_1^{3D}}, \qquad R_D = \frac{D_{11}^{\mathrm{plate}}}{D_{11}^{\mathrm{CLT}}}, \tag{1}$$

where $E_1^A = 1/(h a_{11})$ with $\mathbf{a} = \mathbf{A}^{-1}$, h is the plate thickness, and D_{11}^{CLT} is the bending stiffness of a homogeneous orthotropic plate with the 3-D constants,

$$D_{11}^{\mathrm{CLT}} = \frac{E_1^{3D}\, h^3}{12\,(1 - \nu_{12}\nu_{21})}, \qquad \nu_{21} = \nu_{12}\,\frac{E_2^{3D}}{E_1^{3D}}. \tag{2}$$

For the present SG, symmetry gives $E_2^{3D} = E_1^{3D}$, hence $\nu_{21} = \nu_{12}$. Equation (2) is used here only as a diagnostic reconstruction from the 3-D periodic-solid constants; for an isolated single layer with free outer surfaces it is not, in general, the correct physical reference (Section 3.2).

3.2 Why CLT with 3-D periodic constants is not the single-layer reference

Equation (2) treats the layer as homogeneous, with the 3-D constants at every x_3 and a strain linear through the thickness. Those constants come from an SG periodic in x_3: each fabric layer is bonded to identical neighbours above and below, which restricts the local through-thickness relaxation of the crimped tows. D_{11}^{CLT} is therefore the reference for a layer inside a thick stack, not for an isolated layer. For this crimped plain-weave SG it predicts a higher single-layer bending stiffness than the plate SG, and $R_D < 1$ measures the effect of the free faces, not an error of either model. Stacking restores neighbours to all but the two outer layers, so R_E and R_D should approach unity with the layer count, as reported for plain-weave moduli under aperiodic thickness conditions [2].

Meshes. The single layer (bottom half of the SG, $0.3 \times 0.3 \times 0.02$ mm) is analysed with the original 40×40 voxel grid and 8 elements through its thickness, and with every voxel split $2 \times 2 \times 2$ (16 elements through the thickness). The two-layer SG ($h = 0.04$ mm) is analysed with its original $40 \times 40 \times 16$ grid, with the $2 \times 2 \times 2$ split ($80 \times 80 \times 32$), and with a coarsened $20 \times 20 \times 8$ grid. The coarsened grid is not a subdivision of the original one: its tow volume fraction is 0.510 instead of 0.5225. Stacks of 2, 6 and 10 layers ($h = 0.04$, 0.12 and 0.20 mm) repeat the two-layer SG in phase.

Verification. Nodes, elements, materials and element frames agree with the supplied SG (frames to 3×10^{-16}). For a homogeneous tow block with rotated frames, the 3-D

Table 2: 3-D solid versus classical plate homogenization: single fabric layer (8 and 16 elements through h), supplied two-layer SG (original mesh, 16 elements through h), and the values reported on cdmHUB (SwiftComp, the forum SG). Ratios from Eqs. (1)–(2).

	single layer		two-layer	cdmHUB
	8 el.	16 el.	supplied SG	values
h (mm)	0.02	0.02	0.04	0.0667
E_1^{3D} (GPa)	36.19	35.28	36.19	81.86
E_1^A (GPa)	30.56	29.77	34.68	68.70
R_E	0.8447	0.8438	0.9583	0.839
D_{11}^{plate} (N mm)	0.009838	0.009460	0.1709	0.55
D_{11}^{CLT} (N mm)	0.02444	0.02384	0.1955	2.03
R_D	0.4025	0.3969	0.8741	0.271

C and the plate **A** agree with the closed-form rotated stiffness to 3×10^{-8} and 5×10^{-9} (relative). Re-running the supplied SG reproduces its supplied 3-D solid **C** to 5×10^{-17}. In all plate results $\max|B_{ij}|/(A_{11}h) \le 4\times10^{-12}$ (8×10^{-5} for the coarsened grid), which confirms the mid-plane reference. The single-layer 3-D **C** equals the two-layer one to 2×10^{-16}. This is expected here because the two-layer SG is an exact repetition of two identical halves and both solid homogenizations impose periodicity in x_3.

3.3 Results

Table 2 compares the single layer, the supplied two-layer SG and the values reported on cdmHUB [4]. The two-layer SG gives $R_E = 0.958$ and $R_D = 0.874$: plate stiffnesses only 4 % and 13 % below the 3-D values, far from the forum ratios. The true single layer gives $R_E = 0.845$ and $R_D = 0.403$: the membrane ratio matches the cdmHUB value of 0.839 within 1 %, and the bending reduction is of the same order, though less extreme than the cdmHUB value of 0.271. For this crimped plain-weave SG, the single-layer model reproduces the same qualitative trend seen in the forum data, whereas the supplied two-layer SG does not. The absolute values are not expected to match the forum values because the SG, thickness (0.02 versus 0.0667 mm) and homogenization problem differ; in particular, the plate and 3-D solid SGs are different boundary-value problems. Whether finite-element boundary conditions such as end-face coupling to reference points can by themselves explain the low single-ply D_{11} is examined separately in Section 4; for the present SG, the Abaqus benchmarks in Section 4 also give a low plate D_{11} across the boundary-condition variants tested.

Stacking the layer in phase closes the gap (Table 3, Fig. 5); this table collects the key ratios for the in-phase stacks studied here. R_E rises from 0.845 (1 layer) to 0.958, 0.989 and 0.994 (2, 6, 10 layers), and R_D from 0.403 to 0.874, 1.006 and 1.010; $E_1^{3D} = 36.19$ GPa is the same for every in-phase stack because the x_3-periodic cell does not change. The cdmHUB forum question reports the same trend: plate and 3-D-solid-based results approach each other as plies are added [4]. The slight excess of R_D above unity for 6 and 10 layers follows from the definition of the reference quantity: D_{11}^{CLT} is the bending stiffness of a homogeneous orthotropic plate built from the 3-D constants, whereas the woven stack retains a non-uniform through-thickness stiffness distribution, so R_D need not tend exactly to unity. The sign of the deviation depends on the stacking: mirrored and shifted 6-layer stacks give $R_D = 0.980$ and 0.962.

Table 3: Key ratios for in-phase stacks of the fabric layer, 8 elements per layer; $E_1^{3D} = 36.19$ GPa for every stack.

layers	h (mm)	R_E	R_D	D_{11}^{plate} (N mm)	D_{11}^{CLT} (N mm)	D^{DNS}/D_{11}^{plate}
1	0.02	0.8447	0.4025	0.009838	0.02444	0.989
2	0.04	0.9583	0.8741	0.1709	0.1955	0.993
6	0.12	0.9892	1.006	5.313	5.280	–
10	0.20	0.9936	1.010	24.69	24.44	–

Note: D^{DNS} denotes periodic cylindrical Abaqus bending results (Section 4); '–' means not run. With 16 elements per layer, $R_D = 0.3969$, 0.8717 and 1.005 for 1, 2 and 6 layers, and R_E changes by at most 0.1 %.

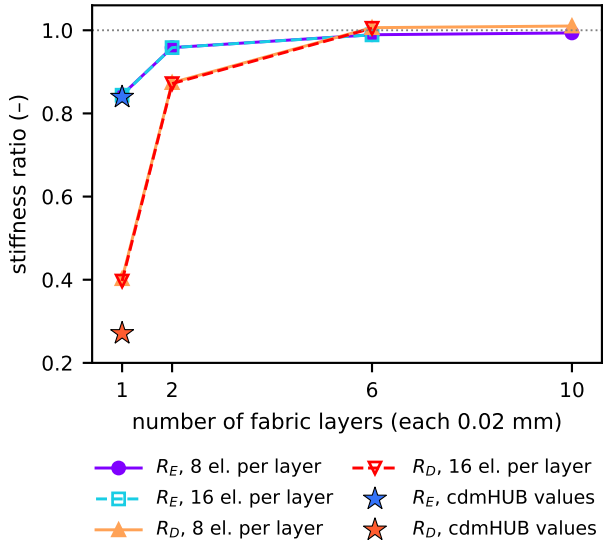


Figure 5: Membrane ratio R_E and bending ratio R_D (Eq. (1)) versus the number of in-phase fabric layers, for 8 and 16 elements per layer; stars: the values reported on cdmHUB for a single ply of the forum SG ($t = 0.0667$ mm). Dotted line: $R = 1$.

Mesh sensitivity. The ratios show limited mesh sensitivity over the meshes tested (Fig. 6). Refining the single layer from 8 to 16 elements through the thickness changes R_E by -0.1 % and R_D by -1.4 %; refining the two-layer SG from 16 to 32 elements changes R_E by less than 0.01 % and R_D by -0.3 %. Absolute values change more: D_{11}^{plate} by -3.8 % and E_1^A by -2.6 % for the single layer, -2.8 % and -2.5 % for the two-layer SG, and E_1^{3D} by -2.5 %. Both refinements split every voxel at fixed voxel geometry and tow fraction, so these $8 \to 16$ and $16 \to 32$ changes are discretization effects. The coarsened two-layer grid also changes the voxelized geometry and the tow fraction; its absolute values lie 1.0–1.4 % below the finest mesh, yet its ratios agree with the finer meshes within 0.3 %. Conclusions are therefore drawn from R_E and R_D; absolute values carry an uncertainty of a few per cent. These results are specific to this crimped plain-weave SG, its in-phase stacking and the thickness range studied here; they should not be generalized to all woven architectures or lay-up arrangements without further analysis.

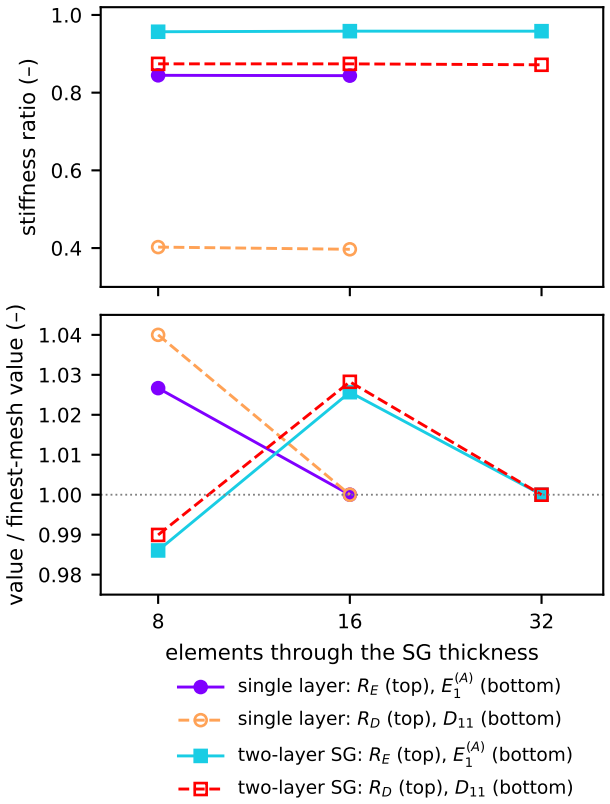


Figure 6: Mesh sensitivity of the plate homogenization. Top: R_E and R_D; bottom: E_1^A and D_{11}^{plate} divided by their finest-mesh values; versus the number of elements through the SG thickness (0.02 mm single layer, 0.04 mm two-layer SG). The 8-element two-layer model is a coarsened grid with tow fraction 0.510 (0.5225 for the others).

4 Direct numerical simulation in Abaqus

The plate SG of the true single layer (Section 3) gives $D_{11} = 0.009838$ N mm, $D_{12} = 0.001343$ N mm and $D_{22} = D_{11}$, i.e. 0.403 of the value $D_{11}^{\text{CLT}} = 0.02444$ N mm reconstructed from the 3-D periodic solid constants. To test whether this low value reflects the bending response of the heterogeneous single layer with free outer surfaces, rather than a numerical artefact of the plate SG, the same layer was bent in Abaqus as a direct numerical simulation (DNS) under three families of boundary conditions: a periodic cell, free-edge coupons loaded by end tractions, and coupons whose end faces are coupled to reference points, matching the type of coupling used in the Abaqus study reported on cdmHUB. No homogenized property enters any of these models; Table 7 (Appendix A) summarizes the model definitions for reproduction, and Fig. 7 shows the boundary conditions as defined in Abaqus.

4.1 Model input

All analyses are linear static (small displacements) in Abaqus/Standard 2024 [7], in N, mm and MPa. The cell is the single layer of Section 2, $L_x \times L_y \times h = 0.3 \times 0.3 \times 0.02$ mm, discretized with the voxel grid and element frames of the plate SG, so that DNS and SG differ only in the boundary-value problem. Coordinates are those of the SG, $x_1, x_2 \in [-0.075, 0.225]$ mm and $x_3 \in [-0.01, 0.01]$ mm, with $x_3 = 0$ at the mid-plane and $x_3 > 0$ towards the top face. A positive curvature κ_{11} stretches the top face ($\varepsilon_{11} = \kappa_{11} x_3$), and a positive M_{11} produces it. The mesh is generated directly from the SG voxelization, one hexahedral element per voxel; the tow and matrix elements form two element sets taken from the voxel material identifiers, each with its own solid section and material.

Mesh. The reference mesh has $40 \times 40 \times 8$ hexahedra per cell (element $0.0075 \times 0.0075 \times 0.0025$ mm; 12 800 elements, 15 129 nodes); the refined mesh splits every voxel $2 \times 2 \times 2$ ($80 \times 80 \times 16$; 102 400 elements, 111 537 nodes). Coupons tile $N \times N$ cells of the reference mesh: $N = 2$, 4 and 8 give 51 200, 204 800 and 819 200 elements (59 049, 233 289 and 927 369 nodes). The supplied two-layer SG ($0.3 \times 0.3 \times 0.04$ mm, $40 \times 40 \times 16$) has 25 600 elements and 28 577 nodes. The tow volume fraction is 0.5225 in every model.

Elements. C3D8 (eight-node brick, full integration with selectively reduced integration of the volumetric terms) is used throughout; C3D8I (incompatible modes) is used once, as a check, for the periodic cylindrical single-layer cell with 8 elements through the thickness.

Materials and orientations. Tows are orthotropic and entered as engineering constants, the matrix as isotropic (Table 1). Each tow element carries its own local material frame through a discrete, element-wise orientation field (coordinate-type orientation with an element-based distribution of two vectors), copied from the yarn frame of its voxel: local axis 1 is the yarn direction vector $\mathbf{a}$ (warp tows along x_1, weft tows along x_2; maximum inclination to the mid-plane 5.7°, measured from the element frames of the SG, Section 2); the second vector $\mathbf{b}$ is the second frame vector, which lies in the fabric plane normal to the yarn. The two vectors are orthonormal to round-off ($|\mathbf{a} \cdot \mathbf{b}| < 10^{-30}$), so the Abaqus construction, local $3 = \mathbf{a} \times \mathbf{b}$ and then local $2 = 3 \times 1$, reproduces the SG frame without any effective re-orthogonalization. The frame is constant within an element and changes element by element at tow cross-overs, with no interpolation or smoothing. The matrix is isotropic and needs no frame.

Solver. One linear static step (no geometric nonlinearity), direct sparse solver, default convergence and output settings. Table 4 summarizes the set-up in Abaqus terms.

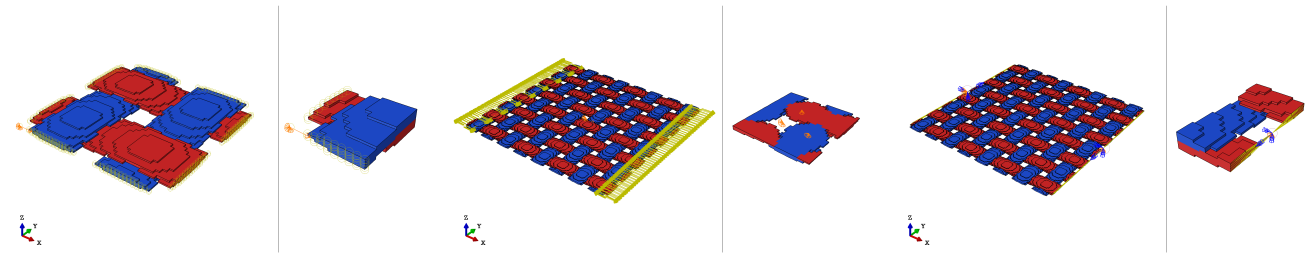
4.2 Boundary conditions and loads

The three set-ups, as defined in Abaqus, are shown in Fig. 7.

Periodic cell. The macroscopic plate displacement for curvatures κ_{11}, κ_{22} is $u_1^0 = \kappa_{11} x_1 x_3$, $u_2^0 = \kappa_{22} x_2 x_3$, $u_3^0 = -(\kappa_{11} x_1^2 + \kappa_{22} x_2^2)/2$, with x_3 measured from the mid-plane; the fluctuation $u - u^0$ is periodic in x_1 and x_2. For a node at $\mathbf{x}$ on the face $x_1 = x_1^{\min}$ and its partner at $\mathbf{x} + L_x \mathbf{e}_1$, and likewise in x_2, this gives the jumps

$$\begin{aligned} &[u_1] = \kappa_{11} x_3 L_x, \quad [u_2] = 0, \quad [u_3] = -\kappa_{11} L_x (x_1 + L_x/2), \\ &[u_1] = 0, \quad [u_2] = \kappa_{22} x_3 L_y, \quad [u_3] = -\kappa_{22} L_y (x_2 + L_y/2), \end{aligned} \tag{3}$$

For each face pair, the node on $x_1 = x_1^{\min} + L_x$ or $x_2 = x_2^{\min} + L_y$ is dependent: with the nodes indexed (i, j, k) on the structured voxel grid ($0 \le i \le n_x$, $0 \le j \le n_y$, $0 \le k \le n_z$; $n_x = n_y = 40$, $n_z = 8$), every node with $i = n_x$ or $j = n_y$ is



(a) (b) (c)

Figure 7: Boundary conditions as defined in Abaqus. Genuine Abaqus/CAE views of the imported input decks; in each panel the whole model (left) and a zoom on the constrained nodes (right); matrix hidden, warp tows red, weft tows blue; triad X, Y, Z $= x_1, x_2, x_3$. (a) Periodic cell ($0.3 \times 0.3 \times 0.02$ mm): orange symbol at the pinned mid-plane corner node; the dummy node carrying the curvature DOFs κ_{11}, κ_{22} is a separate node, coincident with it and attached to no element; yellow circles mark the boundary nodes that enter the periodic constraint equations, the equations themselves (the ties between partner nodes) are not drawn. (b) 4×4-cell coupon ($1.2 \times 1.2 \times 0.02$ mm): yellow arrows on every node of the end faces $x_1 = 0$ and $x_1 = L$, the consistent nodal forces of the linear end traction; orange symbols at the coupon centre, the 3-2-1 supports on three mid-plane nodes (zoom: lower half of the tows only, so the supports show). (c) 4×4-cell coupon: yellow lines from each end face to its reference point at the end-face centroid, the kinematic couplings; orange and blue symbols at the two reference points, their restraints and prescribed rotations UR_2.

Table 4: Abaqus set-up of the DNS models.

Item	Definition
Element	C3D8; C3D8I only as a check (periodic cylindrical cell, 8 elements through the thickness)
Mesh	one element per voxel; 8 elements through the 0.02 mm thickness (16 in the fine check)
Element sets	TOW and MATRIX, from the voxel material identifiers
Orientation	element distribution of two orthonormal vectors with *ORIENTATION (DEFINITION=COORDINATES); local 1 = yarn direction
Periodic cell	*EQUATION per dependent node and DOF, pairs from integer grid indices; jump terms on a dummy node (DOF 1 $= \kappa_{11}$, DOF 2 $= \kappa_{22}$), coincident with the pinned mid-plane node
Traction coupons	*CLOAD consistent nodal forces of $t_1 = \pm c x_3$, exact facet integrals; 3-2-1 *BOUNDARY at mid-plane nodes
RP coupons	*COUPLING with *KINEMATIC on a node-based surface of the whole end face, all DOFs; RP at the end-face centroid; $UR_2 = \pm \kappa L/2$
Outputs	whole-model strain energy; nodal U and RF/RM; element stresses; integration-point coordinates and volumes
Curvature	least-squares quadratic of the nodal u_3 at $x_3 = 0$ over the central gauge cell, averaged across the width

tied to the single independent node $(i \bmod n_x,\ j \bmod n_y,\ k)$, and a node on the shared edge $i = n_x$, $j = n_y$ (corners included) is tied to $(0,0,k)$ by one equation per degree of freedom carrying the sum of both jumps, so no node is constrained twice. The pairs are generated from these integer indices, not by coordinate matching; the count, 729 dependent nodes and 2 187 equations, verifies them. In (3), x_1 and x_2 are the coordinates of the independent node ($x_1 = x_1^{\min}$ on the x_1-pair, $x_2 = x_2^{\min}$ on the x_2-pair), so $[u_3] = -\kappa_{11} L_x \bar{x}_1$ and $-\kappa_{22} L_y \bar{x}_2$ with the pair-midpoint coordinates $\bar{x}_1 = x_1 + L_x/2$, $\bar{x}_2 = x_2 + L_y/2$; this term vanishes only for an origin at the cell centre and is kept here, where $x_1^{\min} = x_2^{\min} = -0.075$ mm. The jumps are imposed as linear *EQUATION constraints, one per dependent node and degree of freedom, $u_i^{\mathrm{dep}} - u_i^{\mathrm{ind}} - c_i \kappa = 0$. The curvatures are the displacement degrees of freedom of a dummy node, DOF 1 $= \kappa_{11}$ and DOF 2 $= \kappa_{22}$, which enter each equation with the coefficient c_i read from (3). With node labels $1 + i + 41(j + 41k)$, the u_1 equation of node 41 ($i = 40$, $j = k = 0$, $x_3 = -0.01$ mm) has three terms and reads `41, 1, 1, 1, 1, -1, 15130, 1, 0.003`: node 41, its partner node 1, and the dummy node 15130 (DOF 1) with $-c_1 = -x_3 L_x = 0.003\,\mathrm{mm}^2$. The dummy node is a separate node attached to no element, placed coincident with the pinned node, at $(-0.075, -0.075, 0)$ mm; because it enters only through the linear constraint equations, its spatial position does not affect the solution. By virtual work its reactions are $R_1 = A M_{11}$ and $R_2 = A M_{22}$, with $M_{\alpha\alpha}$ per unit width and $A = L_x L_y$. Top and bottom faces are traction-free; the mid-plane corner node (label 6725) is pinned ($U_1 = U_2 = U_3 = 0$); together with the periodic constraint equations this removes the rigid-body modes. DOF 1 is prescribed, $\kappa_{11} = 0.1\,\mathrm{mm}^{-1}$, so the curvature is imposed exactly and not fitted; a repeat at $0.05\,\mathrm{mm}^{-1}$ serves only as a linearity check. In the *cylindrical* case DOF 2 is prescribed, $\kappa_{22} = 0$; in the *free anticlastic* case DOF 2 is free, so its reaction $A M_{22}$ vanishes and the cell takes the anticlastic curvature $\kappa_{22} = -(D_{12}/D_{22})\kappa_{11}$.

Traction coupons. $N \times N$ cells, $L = W = 0.3N$ mm, $N = 1$, 2, 4, 8, with $x_1 \in [0, L]$, $x_2 \in [0, W]$ and x_3 measured from the mid-plane, positive up. The linear tractions $t_1 = +c x_3$ on $x_1 = L$ and $t_1 = -c x_3$ on $x_1 = 0$ are applied as concentrated nodal forces (*CLOAD), computed in closed form when the deck is generated as the exact integrals of the bilinear end-face shape functions times the linear traction, so the traction is not lumped piecewise constant per facet. Here $c = 12M/h^3 = 1476\,\mathrm{N\,mm}^{-3}$ for the moment per unit width $M = D_{11} \times 0.1\,\mathrm{mm}^{-1} = 9.838 \times 10^{-4}$ N (the integrated moment reproduces M to ten digits). The sides, top and bottom are free. A 3-2-1 support at three mid-plane nodes (coupon centre: U_1, U_2, U_3; node 0.075 mm from it along x_1: U_2, U_3; node 0.075 mm along x_2: U_3) removes rigid-body motion, with negligible influence on the extracted bending stiffness because the applied end tractions are self-equilibrated and the constrained nodes lie on the mid-plane.

Reference-point coupons. $N = 1$ and 4. Each end face is coupled to a reference point (RP) by a *COUPLING with

*KINEMATIC whose coupling surface is a node-based surface of every node of that end face ($9(40N+1)$ nodes), not an edge node set, with the RP at the end-face centroid, $(x_1,x_2,x_3)=(0,W/2,0)$ or $(L,W/2,0)$; an RP off the mid-plane would add a membrane force to the bending. The coupling includes all three translational and all three rotational DOFs of the RP, whereas the coupled solid nodes carry translations only; because the coupled region is the whole face, the end face stays plane and moves as a rigid body. Rotations $UR_2=\pm\kappa L/2$ with $\kappa=0.1\,\mathrm{mm}^{-1}$ (±0.015 and ±0.06 rad) are prescribed at the two RPs. The left RP has U_1,U_2,U_3,UR_1,UR_3 fixed, the right RP U_2,U_3,UR_1,UR_3; the free U_1 there is an axial roller, so no axial force develops ($|N_{11}|<10^{-16}\,\mathrm{N\,mm}^{-1}$). Sides, top and bottom are free.

4.3 Outputs and stiffness extraction

The outputs are the whole-model strain energy U, the nodal displacements, the reaction forces and moments (dummy-node reactions $R_1=AM_{11}$ and $R_2=AM_{22}$, $A=L_xL_y=0.09\,\mathrm{mm}^2$; RP reaction moment RM_2) and the element stresses. The extracted bending stiffness follows from

$$D=\frac{2U}{A\kappa_{11}^2}=\frac{R_1}{A\kappa_{11}}\quad\text{for the periodic cell, and}\qquad D=\frac{M_{11}}{\kappa_{11}^g}\quad\text{for the coupons.}\tag{4}$$

Here M_{11} is the applied (traction coupons) or reaction (RP coupons) bending moment per unit width, and κ_{11}^g is the curvature fitted over the gauge region. For the cell, D is D_{11} in the cylindrical and $\bar{D}_{11}=D_{11}-D_{12}^2/D_{22}$ in the free anticlastic case; $D_{12}=R_2/(A\kappa_{11})$ in the cylindrical case. In the cell, energy and reaction agree to five digits. The moment obtained by integrating $x_3\sigma_{11}$ over the integration points is 2.1 % lower with C3D8 (0.55 % with 16 elements through the thickness) and agrees to 5×10^{-6} with C3D8I: with the volumetric averaging of C3D8 the integration-point stresses are not the exact work conjugate of the imposed curvature, so D is taken from energy or reaction. For RP coupons $M_{11}=RM_2/W$, with RM_2 the reaction moment at either RP; the two are equal and opposite to all printed digits, and their mean is used. The gauge curvature κ_{11}^g is obtained by least-squares fitting $u_3(x_1)=a_0+a_1x_1-\kappa_{11}^g x_1^2/2$ to the nodal u_3 of the mid-plane nodes ($x_3=0$) of the central cell, $x_1,x_2\in[0.15(N-1),0.15(N+1)]$ mm ($[0.45,0.75]$ mm for $N=4$, $[1.05,1.35]$ mm for $N=8$), away from loaded ends and free sides: at each of its 41 x_1 node positions (spacing 0.0075 mm) u_3 is first averaged over the 41 x_2 positions across the gauge width; κ_{22}^g is obtained analogously from averaging across x_1. For $N=1$ and 2 no interior cell exists and the whole coupon is the gauge, so these results are edge-dominated. Free-edge traction coupons are compared with $\bar{D}_{11}$, RP coupons with D_{11} (Section 4.4).

4.4 Results

Table 5 lists all runs. *Periodic cell.* The cylindrical cell gives $D_{11}=0.009727\,\mathrm{N\,mm}$, 0.989 of the plate SG on the same mesh; halving the curvature to $0.05\,\mathrm{mm}^{-1}$ (linearity check) changes D by less than 10^{-5}. C3D8I gives 0.978 of the plate value, and the refined mesh 0.994. The deflection (Fig. 8a) is the imposed cylindrical surface. The stress

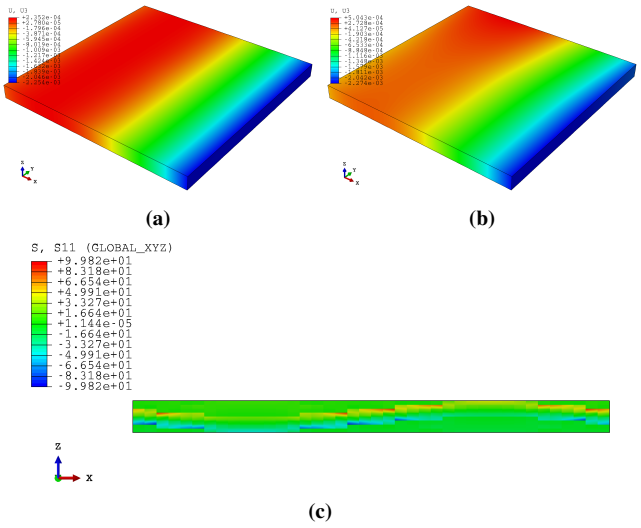


Figure 8: Periodic bending of the single-layer cell ($0.3\times0.3\times0.02$ mm, C3D8, 8 elements through the thickness), $\kappa_{11}=0.1\,\mathrm{mm}^{-1}$: deflection u_3 (mm) on the deformed shape, deformation scale factor 0.3, for (a) the cylindrical case ($\kappa_{22}=0$) and (b) the free anticlastic case ($M_{22}=0$); (c) σ_{11} (MPa, global axes) in the element row along a warp tow, cylindrical case, undeformed, viewed along $-x_2$. Lateral faces constrained by (3), top and bottom traction-free, one mid-plane corner node pinned.

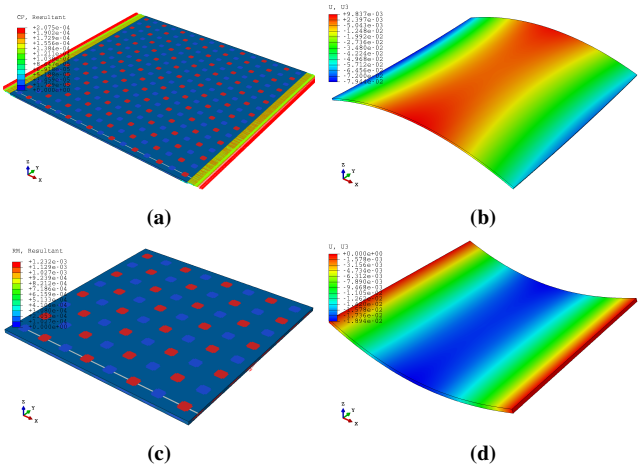


Figure 9: Bending coupons of the single layer (sides, top and bottom free). (a) 8×8-cell traction coupon ($2.4\times2.4\times0.02$ mm), undeformed; warp-tow (red) and weft-tow (blue) crowns on the top surface; symbols on the end faces $x_1=0,L$: consistent nodal forces of the linear end traction (resultant, N); (b) its deflection u_3 (mm), scale factor 3.02. (c) 4×4-cell coupon ($1.2\times1.2\times0.02$ mm) with each end face kinematically coupled to a reference point; reaction-moment symbols (N mm); (d) its u_3 (mm) for end rotations ±0.06 rad, scale factor 6.34.

σ_{11} (Fig. 8c, $|\sigma_{11}|\le99.8$ MPa) is far from linear about the mid-plane: it is concentrated mainly in the crimped warp tow, while the adjacent matrix carries much less axial stress. The cylindrical run gives $D_{12}=0.001167\,\mathrm{N\,mm}$ (C3D8) and 0.001309 N mm (C3D8I) against 0.001343 N mm. The free anticlastic cell (Fig. 8b) settles at $\kappa_{22}/\kappa_{11}=-0.120$, consistent with $-D_{12}/D_{22}$ of the cylindrical run, and gives $D=0.009587\,\mathrm{N\,mm}=0.993\,\bar{D}_{11}$.

Mesh. From 8 to 16 elements through the thickness the DNS D_{11} falls by 3.3 % and the plate-SG D_{11} by 3.8 %, while their ratio moves from 0.989 to 0.994 (Fig. 11). The absolute stiffness depends modestly on the through-thickness discretization, the DNS-to-plate ratio hardly at all,

Table 5: Abaqus DNS of the true single layer (thickness 0.02 mm) and, as a verification check, of the supplied two-layer SG (0.04 mm), $\kappa_{11} = 0.1\,\mathrm{mm}^{-1}$ imposed or, for coupons, measured over the gauge; n_3: elements through the thickness. The reference is the plate-SG stiffness on the same mesh: $D_{11} = 0.009838$ and $\bar{D}_{11} = 0.009655$ N mm ($n_3 = 8$), $D_{11} = 0.009460$ N mm ($n_3 = 16$), $D_{11} = 0.1709$ N mm (two layers). The plate SG gives $-D_{12}/D_{22} = -0.137$. For reference-point coupons the last column reports D/D_{11}, with $D/\bar{D}_{11}$ shown in parentheses only for comparison.

Set-up	Element	n_3	N	κ_{11} (mm^{-1})	κ_{22}/κ_{11}	D (N mm)	Reference	D/reference
Periodic, cylindrical	C3D8	8	–	0.1 imposed	0	0.009727	D_{11}	0.989
Periodic, cylindrical	C3D8	8	–	0.05 imposed	0	0.009727	D_{11}	0.989
Periodic, cylindrical	C3D8I	8	–	0.1 imposed	0	0.009619	D_{11}	0.978
Periodic, cylindrical	C3D8	16	–	0.1 imposed	0	0.009405	D_{11}	0.994
Periodic, free anticlastic	C3D8	8	–	0.1 imposed	−0.120	0.009587	$\bar{D}_{11}$	0.993
Traction coupon, free edges	C3D8	8	1	0.1031	−0.133	0.009539	$\bar{D}_{11}$	0.988
Traction coupon, free edges	C3D8	8	2	0.1029	−0.128	0.009558	$\bar{D}_{11}$	0.990
Traction coupon, free edges	C3D8	8	4	0.1012	−0.122	0.009720	$\bar{D}_{11}$	1.007
Traction coupon, free edges	C3D8	8	8	0.1011	−0.121	0.009729	$\bar{D}_{11}$	1.008
RP-coupled ends, free sides	C3D8	8	1	0.0999	−0.042	0.009835	D_{11}	1.000 (1.019)
RP-coupled ends, free sides	C3D8	8	4	0.0970	−0.034	0.010057	D_{11}	1.022 (1.042)
Two-layer SG, periodic, cylindrical	C3D8	16	–	0.1 imposed	0	0.1697	D_{11}	0.993

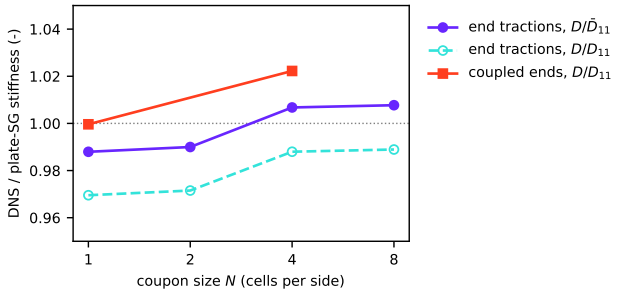


Figure 10: Coupon-size convergence of the DNS bending stiffness of the single layer: traction coupons with free edges, $D/\bar{D}_{11}$ (filled) and D/D_{11} (open); coupons with end faces coupled to reference points, D/D_{11}. Plate-SG values: $D_{11} = 0.009838$, $\bar{D}_{11} = 0.009655$ N mm. For $N = 1$, 2 the gauge is the whole coupon.

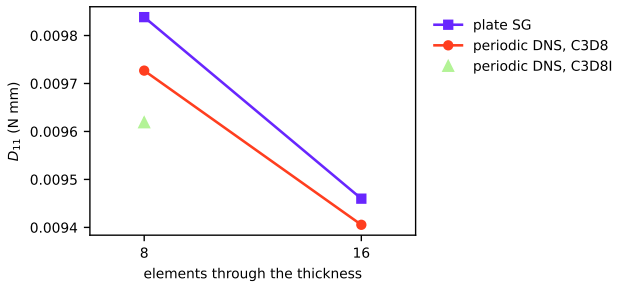


Figure 11: Through-thickness refinement of the single layer (0.02 mm): plate-SG D_{11} and periodic cylindrical DNS D_{11} (C3D8; C3D8I at 8 elements) for 8 and 16 elements through the thickness.

so 8 elements suffice for this comparison.

Two-layer SG (verification check). Outside the single-layer benchmark, the same periodic DNS of the supplied two-layer SG gives 0.1697 N mm against 0.1709 N mm from its plate SG (0.993). After normalization by h^3, the two-layer plate SG is 2.17 times stiffer than the single-layer one (2.18 from the DNS), showing that, for this crimped plain-weave SG, stacking changes the through-thickness distribution of the effective stiffness and not only the geometric h^3 factor.

Traction coupons. The coupons bend anticlastically (Fig. 9b) with κ_{22}/κ_{11} between −0.133 and −0.121, close to $-D_{12}/D_{22} = -0.137$ of the plate SG. The gauge stiffness is 0.988 and 0.990 of $\bar{D}_{11}$ for the edge-dominated $N = 1$ and 2 and 1.007 and 1.008 for $N = 4$ and 8 (Fig. 10): with an interior gauge cell the estimate has converged to 0.1 %, and a free-edge coupon of the single layer bends with the plate-SG stiffness $\bar{D}_{11}$.

Reference-point coupons. Coupling an end face to a reference point by a kinematic surface coupling constrains that face to move as a rigid plane, which suppresses the anticlastic curvature near the ends: κ_{22}/κ_{11} drops to −0.042 ($N = 1$) and −0.034 ($N = 4$), and the response is governed by D_{11} rather than $\bar{D}_{11}$ (Table 5). The gauge stiffness is 1.000 and 1.022 of D_{11} (1.019 and 1.042 of $\bar{D}_{11}$). The additional 2 % at $N = 4$ is consistent with an end-constraint boundary-layer effect: the rigidized end faces suppress local warping and alter the curvature field near the grips, so the central-cell fit returns a slightly higher stiffness. Taking the nominal curvature $2|UR_2|/L = 0.1\,\mathrm{mm}^{-1}$ from the end rotations instead of the gauge curvature gives $D = 0.009828$ and 0.009758 N mm (0.999 and 0.992 of D_{11}), so in this benchmark the curvature definition changes D by less than 3 %.

4.5 What the boundary conditions show

For the true single layer, all DNS cases considered here give D close to the corresponding plate-SG comparator: within about ±2.2 % on a like-for-like basis (D_{11} for cylindrical or RP-coupled cases, $\bar{D}_{11}$ for free-anticlastic or free-edge cases). If the RP coupons are instead compared with $\bar{D}_{11}$, the difference rises to +4.2 %. All DNS values remain far below the CLT value reconstructed from the 3-D periodic solid constants, at about 0.39 to 0.41 of $D_{11}^{\mathrm{CLT}} = 0.02444$ N mm (0.02384 N mm on the refined mesh); even the stiffest coupon would need a further factor 2.43 to reach it. In this benchmark, reference-point coupling altered the inferred single-layer bending stiffness by only a few per cent. These results do not support explaining the much larger cdmHUB discrepancy by the reference-point coupling boundary conditions alone (Section 5). The DNS does not rank the two SGs: for this crimped plain-weave SG it identifies the plate SG with free-surface bending of the true single layer, and the 3-D periodic solid SG with a different boundary-value problem.

The set-up details that change the extracted D in such a study are: (i) one constraint equation set per dependent node, with edge and corner nodes tied once; (ii) D from en-

ergy or reaction, not from integration-point stresses of C3D8 (2.1 % low here); (iii) compare cylindrical or RP-coupled cases with D_{11}, and free-anticlastic or free-edge cases with $\bar{D}_{11}$; (iv) moment per unit width, RM_2/W, and gauge curvature measured away from the ends; (v) model the actual heterogeneous layer with per-element yarn orientations at the true single-layer thickness; first verify that the model contains only one fabric layer and not inadvertently more than one; replacing it by a homogeneous solid built from 3-D effective constants answers a different problem, and thickness errors strongly affect D through the approximate h^3 scaling.

5 Why the models disagree: prospective modelling causes to check

5.1 Comparison with the values reported on cdmHUB

For this crimped plain-weave SG, the true single layer gives $R_E = 0.845$ and $R_D = 0.403$ with 8 elements through the thickness; with 16 elements the values are $R_E = 0.844$ and $R_D = 0.397$, against 0.839 and 0.271 on cdmHUB (Table 2). The membrane ratio is closely matched; the bending reduction is of the same order but less extreme: $D_{11}^{\mathrm{CLT}}/D_{11}^{\mathrm{plate}} = 2.48$ here and 3.69 on cdmHUB. The two SGs differ in thickness (0.02 versus 0.0667 mm), yarn geometry and crimp, so only the ratios are compared, and the trend, not exact agreement, is claimed. This is consistent with the cdmHUB observation that the plate and 3-D-solid-based values move closer as plies are added. CLT built from the 3-D periodic solid constants does not represent the same boundary-value problem as the isolated Kirchhoff plate SG and, for this crimped plain-weave SG, predicts a higher bending stiffness for a single isolated layer. In this benchmark, all Abaqus models of the same heterogeneous true single layer give 0.39–0.41 of D_{11}^{CLT} (Table 5), whereas the Abaqus value reported on cdmHUB is $2.17/2.03 = 1.07$ of the corresponding CLT value reported there.

5.2 Can the coupling boundary conditions explain a factor of four?

The cdmHUB follow-up asks whether the reference-point coupling of the Abaqus model explains $2.17/0.55 = 3.95$. Here the question is tested only within the present benchmark geometry and material model, not as a universal statement about all coupled-end coupon models. In the coupled single-layer coupons of Section 4, each end face, as a node-based surface containing all its nodes, was kinematically coupled (rigid *KINEMATIC coupling, not a distributing coupling) to a reference point located at the centroid of that end face; the imposed rotations were $\pm\kappa L/2$ about the x_2 axis with $\kappa = 0.1$ mm^{-1}; the left reference point was fixed in all other DOFs and the right one left free only in U_1, so no net axial force develops; the side faces and the outer top and bottom faces were traction-free; no periodic constraints were applied. The reference-point-coupled coupons gave $D_{11} = 0.009835$ N mm for the 1×1-cell coupon and 0.01006 N mm for the 4×4-cell coupon, 1.000 and 1.022 of the plate value, whereas free-edge coupons under linear end tractions gave 0.970–0.989 of the plate value (0.988–1.008 of $\bar{D}_{11}$), and the periodic unit-cell bending result was 0.989 of the plate value. In this benchmark, reference-point coupling restrains anticlastic curvature and end-section warping. The anticlastic contribution is quantified here by $D_{11}/\bar{D}_{11} = 1.019$, and the remaining difference is attributable to end effects on short coupons; reaching D_{11}^{CLT} would need a factor of 2.48 from the plate value and 2.43 from the stiffest coupon.

For the SG studied here, a true single-layer DNS with free outer surfaces does not support a bending stiffness near the CLT value reconstructed from 3-D periodic solid constants; if a different study obtains such a value, the SG definition (in particular whether the model actually contains more than one fabric layer), thickness interpretation, constitutive representation, discretization, boundary conditions, and stiffness-extraction procedure should be checked. Table 6 lists these prospective causes, with the symptom each produces and the check that exposes it, ordered by the authors' judgment for the present discrepancy. Causes 1 and 2 can readily produce a factor-of-four discrepancy on their own; cause 3 can also do so in general if moment, width normalization, thickness, or curvature are defined inconsistently, although that magnitude was not observed in the present benchmark. Causes 4–6 matter only when severe, and the coupling (cause 7) changes D_{11} by only a few per cent in this benchmark. Magnitudes not measured here are estimates, not results of this study.

Additional practical checks. Each of the following leaves a recognizable symptom. (i) Mixed units (N mm versus N m, mm versus m in geometry or moduli): factors of 10^3 or 10^6; audit the units of geometry, moduli, reaction moments and the reported D_{11}. (ii) A thickness in Eq. (2) different from the modelled one: the CLT reference is off by the cube of the thickness ratio although the FEM is correct; use the same h in every model and formula. (iii) A shell or composite-layup model in place of the tow/matrix solid: the result follows the shell input, not the yarn-scale mechanics; check the element family and section definition. (iv) A reference point off the mid-surface: a non-zero N_{11} during nominal pure bending; check the RP coordinates and N_{11} in the gauge. (v) Geometric nonlinearity switched on: D_{11} depends on the curvature level; repeat at half the curvature, or linear, as done here (Table 5). (vi) Extension–bending coupling ignored in an unsymmetric SG or stack: membrane strains appear in bending and M_{11}/κ_{11} is contaminated; check $B \approx 0$ and $N_{11} \approx N_{22} \approx 0$. (vii) Duplicate periodic equations at edges and corners: an over-constrained cell, solver warnings or a stiffer response; tie every dependent node once.

5.3 Limitations

- The SG and Abaqus model of the cdmHUB forum question were not available for direct reproduction; the benchmark SG differs from that SG, and its layer is 0.02 mm thick against 0.0667 mm, so R_E and R_D are compared, not absolute stiffnesses.
- The yarn geometry is voxel-based (stair-stepped); the analyses are linear elastic with small deformations.
- R_E is inferred from homogenization only; no direct membrane DNS benchmark was performed for the true

Table 6: Prospective causes of a discrepancy in a single-ply heterogeneous FEM bending model, ordered by the authors' judgment of plausibility for the present discrepancy, not by a quantified probability. Stiffness values refer to the 0.02 mm single layer of this study; plate $D_{11} = 0.009838$ N mm, $D_{11}^{\mathrm{CLT}} = 0.02444$ N mm; A: planform area of the model ($L_x L_y$ for the periodic cell, $A = WL$ for a coupon).

#	Prospective cause	Expected symptom and magnitude	Check that exposes it	What this study shows
1	Not a true single layer, or different thicknesses in the plate SG, the FEM model and the stiffness extraction	$D_{11} \propto h^3$: a thickness ratio of 1.58 alone gives 4×. A hidden second layer brings the plate result close to CLT and to the FEM, and the gap reappears only when the SG is split	Count warp and weft runs per in-plane column through the thickness; use one h in all models; compare D_{11}/h^3	The supplied 0.04 mm SG held two identical layers (each tow family once in each half of a column, no tow crossing the mid-plane): $R_D = 0.874$ versus 0.403 for the true layer
2	FEM model representing the thickness-periodic 3-D solid problem rather than the isolated heterogeneous single layer, e.g. by using homogenized 3-D constants or by imposing thickness-periodic constraints	The FEM result moves toward the CLT value reconstructed from the 3-D periodic solid constants; for the cdmHUB numbers, $2.17/2.03 = 1.07$, with any excess plausibly due to end effects or extraction details	Inspect the material and section assignment: separate tow and matrix regions with per-element yarn frames, traction-free top and bottom faces, no constraint equations between them	The heterogeneous single layer with free faces gives 0.39–0.41 of D_{11}^{CLT} (0.0095–0.0101 versus 0.02444 N mm)
3	Moment or curvature extraction	In general can bias D_{11} by 2–4× in an otherwise correct model if moment, width normalization, thickness or curvature are defined inconsistently (not observed at that magnitude here), with energy and moment estimates disagreeing. Using total bending moment instead of moment per unit width makes the reported quantity scale with width and carry units of N mm rather than N; the inferred D_{11} is then too large by a factor $W/(1\ \mathrm{mm})$ if width is left in millimetres; wrong area in $2U/(A\kappa^2)$: error $A_{\mathrm{true}}/A_{\mathrm{used}}$; curvature from end rotations over coupled ends: a few per cent; C3D8 integration-point sum of $x_3\sigma_{11}$: about 2 % low	Compute D_{11} from $2U/(A\kappa^2)$ and from M_{11}/κ with M_{11} per unit width (N); a constant factor between them exposes a geometric error; take κ from a central gauge fit	$2U/(A\kappa^2)$ and $RF_1/(A\kappa)$ agree to five digits; gauge and end-rotation curvature differ by 3.1 % (4 × 4-cell coupled coupon: 1.022 versus 0.992 of plate D_{11}); C3D8 moment sum 2.1 % low
4	Too few elements through the thickness, or element type	Too few elements through the thickness can bias the bending stiffness substantially; the sign is problem-dependent (element formulation, aspect ratio, mesh distortion) and must be checked by refinement. Reduced-integration bricks also require an hourglass-energy check	Refine through the thickness at a fixed in-plane mesh (1, 2, 4, 8, 16 elements); compare C3D8, C3D8I and C3D8R, with the hourglass energy small against the strain energy	8 to 16 elements: DNS D_{11} −3.3 %, plate D_{11} −3.8 %, R_D 0.403 → 0.397; C3D8I 1.1 % below C3D8
5	Material frames not following the yarn path	Frames ignoring crimp: too stiff, up to tens of per cent; frames missing altogether (axis 1 along x_1 in every tow) align the weft fibres with x_1 and grossly over-stiffen	Plot the element material triads against the yarn tangent; rerun with frozen global frames to measure the sensitivity	Frames from per-element orientation vectors of the SG; orientation check against the prescribed yarn-tangent field to machine precision
6	Different SGs in the plate and FEM models	R_E, R_D not reproducible; 3-D constants of the FEM SG differ from those used in CLT; magnitude set by geometry, tow fraction and crimp	Use one mesh, material set and frame field in both models; compare tow fraction, crimp angle and h; reproduce the 3-D constants with both	One mesh and frame field in both codes (tow fraction 0.5225, crimp up to 5.7°); the re-run reproduces the supplied 3-D solid homogenization result for the same SG
7	End faces coupled to reference points (the follow-up hypothesis)	Restrains anticlastic curvature and end warping: slightly too stiff in this benchmark; larger effects would require additional over-constraint and are not quantified here	Repeat with free-edge linear end tractions and with a periodic cell; vary the coupon length; use gauge curvature	1.000 (1 × 1 cells) and 1.022 (4 × 4 cells) of plate D_{11}; $D_{11}/\bar{D}_{11} = 1.019$; free-edge coupons 0.970–0.989

single layer.

- Coupon curvature uses a one-cell gauge estimator (the whole coupon for 1 × 1 and 2 × 2 cells, where the free edges dominate).
- Absolute D_{11} changes by about 4 % between 8 and 16 elements through the thickness; R_E and R_D change by at most 1.4 %.
- The layer trend uses in-phase stacking only.

6 Conclusions

1. The supplied 0.04 mm SG contains two identical in-phase fabric layers; in this benchmark, the corresponding true single layer is taken as one half of that thickness, 0.02 mm.

2. For this crimped plain-weave SG, the true single-layer Kirchhoff plate gives $R_E = 0.845$ and $R_D = 0.403$, reproducing the trend reported on cdmHUB in the sense

that R_E is closely matched and R_D shows a bending reduction of the same order, though less extreme (0.839, 0.271 on cdmHUB); the discrepancy in R_D decreases as identical in-phase layers are stacked ($R_D = 0.874$, 1.006, 1.010 for 2, 6 and 10 layers).

3. Abaqus DNS of the same heterogeneous true single layer with free outer surfaces gives D_{11} within about 1 % of the plate value for the periodic unit-cell bending case and within about 3 % for the free-edge and reference-point-coupled coupon models; thus, in this benchmark, a true single-layer DNS with free outer surfaces does not support a bending stiffness near the CLT value reconstructed from 3-D periodic solid constants.
4. In the present benchmark, reference-point coupling changes the single-layer D_{11} by at most 2.2 % and therefore cannot by itself explain an approximately fourfold discrepancy.
5. Accordingly, a single-ply FEM bending stiffness near the CLT value would point to the SG definition, thickness interpretation, constitutive representation based on homogeneous 3-D periodic solid constants, discretization, or the stiffness-extraction procedure; Table 6 gives corresponding checks for these possibilities.

Future work. A periodic membrane DNS of A_{11} would check R_E directly. Smooth (non-voxel) yarn geometry, a reconstruction of the cdmHUB SG and Abaqus set-up, coupons with 16 elements through the thickness, reference-point coupons of 8×8 cells, and thickness and period scans would extend the benchmark. A controlled cross-check should isolate these factors, varying only the SG thickness definition, layer phasing, constitutive representation, discretization and stiffness-extraction method within the same benchmark geometry and boundary conditions.

Use of AI tools

CompositesAI [5] led the study: planning, model and boundary-condition specification, interpretation and review. Claude Code served as the agentic distribution channel that dispatched the tasks to computational agents running OpenSG and Abaqus and relayed queries and results. OpenSG and Abaqus performed all reported computations; the CompositesAI consultations are recorded in [8–12]. The authors reviewed the content and take full responsibility for it.

References

[1] Wenbin Yu. A unified theory for constitutive modeling of composites. *Journal of Mechanics of Materials and Structures*, 11(4):379–411, 2016.

[2] Xin Liu, Khizar Rouf, Bo Peng, and Wenbin Yu. Two-step homogenization of textile composites using mechanics of structure genome. *Composite Structures*, 171:252–262, 2017.

[3] Khizar Rouf, Xin Liu, and Wenbin Yu. Multiscale structural analysis of textile composites using mechanics of structure genome. *International Journal of Solids and Structures*, 136–137:89–102, 2018.

[4] cdmHUB forum. Discrepancy between SwiftComp 2D and 3D homogenization for thin plain-weave composites. Forum thread with replies, cdmHUB (Composites Design and Manufacturing HUB), https://cdmhub.org. Accessed October 2026.

[5] CompositesAI. Consultation on the cdmHUB thin plain-weave plate question: study plan, verdict and follow-up. https://compositesai.com/c/cf185e6c-763b-4708-af22-15c321f1e015, 2026. Chat of 21–22 October 2026.

[6] wenbinyugroup. OpenSG: open-source structure genome code. https://github.com/wenbinyugroup/OpenSG, 2026. Commit f31b196.

[7] Dassault Systèmes. Abaqus 2024 documentation. Dassault Systèmes Simulia Corp., Johnston, RI, USA, 2024.

[8] CompositesAI. Why plate and 3-D solid homogenization differ for a thin crimped plain weave, and the sign of small bending-ratio deviations. https://compositesai.com/c/26c488d7-cbd8-49c1-b649-8eda98cb4f36, 2026. Chat of 22 October 2026.

[9] CompositesAI. Comparator and boundary-condition effect for reference-point-coupled bending coupons. https://compositesai.com/c/6c7a7738-6c60-4ce8-8b71-df7911fa90ba, 2026. Chat of 22 October 2026.

[10] CompositesAI. Stiffness extraction with C3D8 and through-thickness mesh dependence of the bending DNS. https://compositesai.com/c/076d0a20-5b31-4fce-b3b1-498a95ff54a1, 2026. Chat of 22 October 2026.

[11] CompositesAI. Expected symptoms and magnitudes of modelling errors in single-ply woven bending models. https://compositesai.com/c/127bf286-50df-456a-afdf-402df1f1dcc9, 2026. Chat of 22 October 2026.

[12] CompositesAI. Review of the conclusions on the cdmHUB thin plain-weave plate question. https://compositesai.com/c/fe00a736-a5c9-4c65-9e07-e766c240f891, 2026. Chat of 22 October 2026.

A Data and reproducibility

The supplementary package contains the inputs, scripts and outputs needed to reproduce every number, table and figure of this report. It is organised in six folders. (i) Inputs: the supplied SG in OpenSG and SwiftComp formats, its supplied 3-D solid result and the constituent data of Table 1. (ii) Homogenization: the input and output of every OpenSG solid and plate run (all meshes, the single layer and the stacks), the SG audit and layer check, the orientation and solver checks, and the OpenSG source pinned at commit f31b196 [6]. (iii) Abaqus: for each simulation the input deck, a metadata record (node, element and grid counts, curvature or load, constraints) and the solver status and message files; the one deck larger than 100 MB

Table 7: Abaqus model summary (Abaqus/Standard 2024, N–mm–MPa, one linear static step without geometric nonlinearity, direct sparse solver).

Item	Definition
Mesh and elements	One C3D8 element per SG voxel; $n_3 = 8$ per 0.02 mm layer (cell: $41 \times 41 \times 9 = 15{,}129$ nodes); checks on the periodic cylindrical cell only: C3D8I at $n_3 = 8$, $n_3 = 16$ (voxels split $2 \times 2 \times 2$), and $\kappa_{11} = 0.05\,\mathrm{mm}^{-1}$ for linearity
Sets, sections	Tow and matrix element sets from the voxel material identifiers; one solid section each; tow orthotropic (engineering constants), matrix isotropic
Orientation	Rectangular coordinate-type *ORIENTATION, one per tow element (element distribution): local 1 along the yarn direction vector **a**; local 2 in the plane of **a** and the second frame vector **b**, orthogonalized to local 1; local 3 = local 1 × local 2; constant within an element
Periodic cell	*EQUATION per dependent node and DOF; dependent nodes on $x_1 = x_1^{\min} + L_x$ or $x_2 = x_2^{\min} + L_y$, independent node $(i \bmod n_x, j \bmod n_y, k)$ from the integer grid indices, so an edge or corner node carries one equation set with both jumps; dummy node (separate node outside the mesh, coincident with the pinned node) DOF 1, 2 = κ_{11}, κ_{22} with coefficients $x_3 L_x$, $x_3 L_y$, $-L_x(x_1^{\min} + L_x/2)$, $-L_y(x_2^{\min} + L_y/2)$; e.g. at $x_3 = -h/2$, $L_x = 0.3$ mm, the U_1 equation is $u_1^{\mathrm{dep}} - u_1^{\mathrm{ind}} + 0.003\,u_1^{\mathrm{dum}} = 0$, where $u_1^{\mathrm{dum}} = \kappa_{11}$; one mid-plane node pinned (U_1–U_3); $\kappa_{11} = 0.1\,\mathrm{mm}^{-1}$ prescribed; $\kappa_{22} = 0$ prescribed (cylindrical) or free (anticlastic); the two-layer SG cell is a verification case only
Traction coupon	*CLOAD: consistent nodal forces of $t_1 = +c\,x_3$ ($x_1 = L$) and $-c\,x_3$ ($x_1 = 0$), integrated in closed form on the bilinear facets when the deck is generated; $c = 12 M_{11}/h^3$, $M_{11} = 9.838 \times 10^{-4}$ N; mid-plane supports U_1–U_3, U_2–U_3, U_3
RP coupon	*COUPLING with *KINEMATIC on a node-based surface of all nodes of the entire end face, all DOFs; RPs at $(0, W/2, 0)$ and $(L, W/2, 0)$; $UR_2 = \pm\kappa L/2$, $\kappa = 0.1\,\mathrm{mm}^{-1}$; left RP $U_1, U_2, U_3, UR_1, UR_3$ fixed, right RP U_2, U_3, UR_1, UR_3 fixed
Output	Whole-model strain energy, nodal U, RF/RM, element stresses
Extraction	Cell: $D = 2U/(A\kappa_{11}^2) = R_1/(A\kappa_{11})$; coupons: $D = M_{11}/\kappa_{11}^g$, M_{11} applied moment per unit width or $\lvert RM_2\rvert/W$ averaged over the two RPs (equal and opposite); κ_{11}^g from a least-squares fit $u_3 = a_0 + a_1 x_1 - \kappa_{11}^g x_1^2/2$ to the nodal mid-plane ($x_3 = 0$) values of u_3, after averaging over x_2 at each x_1. For $N = 4$, 8, the fit uses the central SG-cell gauge region $\lvert x_1 - L/2\rvert \le L_{\mathrm{cell}}/2$, $\lvert x_2 - W/2\rvert \le W_{\mathrm{cell}}/2$, where $L_{\mathrm{cell}} = L_x$ and $W_{\mathrm{cell}} = L_y$; for $N = 1$, 2, it uses the whole coupon.

is regenerated by its script. (iv) Scripts: model generation, run and post-processing scripts, all with paths relative to the package root. (v) Results: the tables of all three stages of the study in machine-readable and text form. (vi) Figures: the Abaqus/CAE images with their deformation scale factors, and the data plots. A guide at the package root defines every quantity, and a SHA-256 checksum list covers every file. Software: OpenSG (Python 3.13, JAX 0.11.1 in 64-bit floating point), Abaqus/Standard and Abaqus/CAE 2024 [7], NumPy 2.5.2 and Matplotlib 3.11.1 for post-processing. Units are N, mm and MPa throughout: A in N/mm, D in N mm, moduli in GPa, curvature in 1/mm. The CompositesAI consultation record is available separately.

Table 7 collects the Abaqus model definitions of Section 4.

B CompositesAI review provenance: major changes made

CompositesAI reviewed each section and then the full report; the blocker (B) and major changes made are listed below.

Sections 1–2 (introduction, SG). • Plate and 3-D solid routes stated as different boundary-value problems; "can give similar" stiffnesses for thick laminates. • Scope limited to an SG of the same kind, not the unavailable forum SG. • Ply-count observation kept, attributed to the cdmHUB forum question. • Crimp defined as the maximum inclination of the yarn axis to the mid-plane, from the element frames. • Tow shown orthotropic, not transversely isotropic (G_{23} check). • Single-ply reading of the SG called misleading, not wrong; the SG and its 3-D properties internally consistent; the source citation attached. • Two-layer finding phrased as an in-phase stack that x_3-periodic homogenization does not distinguish; column test rewritten. • Single layer defined as the bottom half with original materials and frames, $h = 0.02$ mm in all models. • S_{11} sign change described within the individual tow; forward reference to the Abaqus specification.

Section 3 (homogenization). • Free-face mechanism softened; the gap decreases, not vanishes, with stacking. • Identity of the 3-D **C** explained by exact repetition and x_3 periodicity. • Results framed as the same qualitative trend; different boundary-value problems; forward reference to the Abaqus check. • Table caption lists both single-layer meshes; "limited" mesh sensitivity; scope-limitation sentence added.

Section 4 (Abaqus DNS). • **(B)** RP placed at the end-face centroid, $(0, W/2, 0)$ and $(L, W/2, 0)$, with *COUPLING and *KINEMATIC over the whole end face; RP and solid-node DOFs stated. • Coupling matched in type, not a reproduction of the cdmHUB model. • Mesh one element per voxel; tow and matrix sets from the voxel material identifiers. • Orientation field defined (axes 1, 2, 3), constant per element at tow cross-overs. • *EQUATION constraints, independent-node rule, no double constraints at edges and corners. • $[u_3]$ jump stated as constant over each face pair (the suggested form was corrected). • Traction sign, exact consistent nodal forces (*CLOAD) and support wording. • M_{11} per unit width in Eq. (4); least-squares gauge fit and its sampling. • Stress-field, stacking, rigid-plane and end-effect statements toned down. • Like-for-like comparators; coupling alone not supported as the cause; checklist item on the true heterogeneous layer. • Abaqus model summary added (Table 7).

Sections 5–6 (causes, conclusions). • **(B)** Table 6, row 2: FEM of the thickness-periodic problem, no "by construction" claim. • CLT from 3-D periodic constants stated as a different boundary-value problem. • Abaqus ratio $2.17/2.03 = 1.07$; coupling test limited to this benchmark. • Coupled-coupon definition (centroid RP, rigid coupling, axial release); ratios referenced to the plate value; anticlastic part "quantified", not "bounded". • Checks list adds boundary conditions and a hidden second layer. • Area A defined; total-moment units corrected; element-type magnitudes made qualitative. • Limitation on R_E, conclusions 1–3 and future work tightened.

Full report [5]. • **(B)** CLT with the 3-D periodic constants, Eq. (2), stated as a diagnostic reconstruction, not the physical reference for a single layer with free outer surfaces. • **(B)** Periodic-node rule after Eq. (3): dependent node on the $x_1^{\min} + L_x$ or $x_2^{\min} + L_y$ face, tied to its grid-index partner; one combined equation set at shared edges and corners. • **(B)** Factor of four claimed only for causes 1 and 2; for extraction errors (cause 3) only in general, not observed in this benchmark. • **(B)** Chat records [8–12] no longer cited as evidence; physics and modelling claims rest on the report's results and the literature. • Mesh sensitivity: the $8 \to 16$ and $16 \to 32$ changes are discretization effects at fixed voxel geometry; only the coarsened two-layer grid also changes the voxel geometry and tow fraction. • Two-ply reading of the SG "consistent with" the source publication, not "agrees with". • Abaqus reproducibility: orientation orthogonalization, index-based periodic pairing with an example equation, separate dummy node, gauge bounds and mid-plane sampling, whole-face coupling, moment from both RPs, and the scope of the checks (Table 7). • Limitation added: the forum SG and Abaqus model were not available for direct reproduction.